Ultrasonics 108 (2020) 106017

Contents lists available at ScienceDirect

Ultrasonics

journal homepage: www.elsevier.com/locate/ultras

An amplitude prediction model for a giant magnetostrictive ultrasonic transducer

Huilin Zhou[a], Jianfu Zhang[a,b,*], Pingfa Feng[a,b,c], Dingwen Yu[a], Zhijun Wu[a]

[a] Beijing Key Lab of Precision/Ultra-precision Manufacturing Equipments and Control, Department of Mechanical Engineering, Tsinghua University, Beijing 100084, China
[b] State Key Laboratory of Tribology, Department of Mechanical Engineering, Tsinghua University, Beijing 100084, China
[c] Division of Advanced Manufacturing, Tsinghua Shenzhen International Graduate School, Tsinghua University, Shenzhen 518055, China

ARTICLE INFO

Keywords:
Giant magnetostrictive ultrasonic transducer
Equivalent stiffness
Mechanical quality factor
Odd power amplitude prediction

ABSTRACT

Rotary ultrasonic machining (RUM) is widely used in the processing of brittle and hard materials. The application of giant magnetostrictive ultrasonic transducers (GMUT) with effective vibration performance is an increasingly popular field of research within RUM. A generalized amplitude prediction model for GMUT is obtained in this paper by first providing an equivalent kinetics model of the GMUT. Considering the influence on interaction force between Terfenol-D and the external mechanical mechanism, the prestress mechanism of Terfenol-D and the joint face of the horn are determined as equivalent to two spring-damping systems in series, and a general GMUT vibration equation is established. The equivalent stiffness of the prestress mechanism is then identified, and the mechanical quality factor of the vibration system is calculated by impedance analysis. The influence of the joint face of the horn and the prestress mechanism on the amplitude is then studied by nonlinear least square fitting. Based on a magnetostriction and magnetization model, an odd power amplitude prediction model with mechanical quality factor, excitation current amplitude, and excitation frequency is proposed. The experimental results demonstrate that the proposed model can effectively predict the output amplitude of the GMUT with different mechanical quality factors for different excitation signals, providing a method for system design and optimization of the GMUT.

1. Introduction

Rotary ultrasonic machining (RUM) is widely used in the machining of brittle and hard materials and composite laminates, most notably in milling [1] and drilling [2,21]. Piezoelectric transducers have traditionally been utilized to create the ultrasonic vibrations in RUM, however, giant magnetostrictive materials [3,4] are now being considered for this role. Giant magnetostrictive ultrasonic transducers (GMUT) have undergone extensive recent development, and possess numerous advantages over the piezoelectric materials, including a large magnetostrictive coefficient, high power capacity, fast response speed, and the ability to produce a large ultrasonic vibration amplitude output [5,6]. As such, the application of GMUT combined with giant magnetostrictive materials (such as Terfenol-D) as vibrators in RUM has become a popular field of research.

Numerous scholars have studied the amplitude output characteristics of the GMUT, presenting a number of theoretical models, including the domain theory model and equivalent circuit model. Dapino et al. [7] found that the measured strain of the GMUT was related to the moment rotation of the material in the applied field and the elastic properties of the material. W Huang et al. [8] established the magnetoelastic dynamic strain model of the GMUT based on the Jiles Atherton model and kinetics theory. Wakiwaka H et al. [9] established a mechanical vibration model by electrical impedance analysis. Based on the equivalent circuit, Cai W et al. [10–12] presented a bilateral capacitance compensation method and a vibration amplitude model for the giant magnetostrictive ultrasonic processing system, and discussed the effect of the temperature on the performance of the GMUT.

Due to the complex multi-physical field coupling characteristics of giant magnetostrictive materials, the universal amplitude prediction model and amplitude stability of the GMUT remain key issues to be explored. The vibration performance of the GMUT is closely related to its prestress states, including the prestress states of Terfenol-D and the joint face of the horn. Therefore, it is important to take factors such as the prestress mechanisms of the Terfenol-D and the joint face of the horn into account when establishing a universal amplitude prediction

* Corresponding author at: Beijing Key Lab of Precision/Ultra-precision Manufacturing Equipments and Control, Department of Mechanical Engineering, Tsinghua University, Beijing 100084, China.
E-mail address: zhjf@tsinghua.edu.cn (J. Zhang).

https://doi.org/10.1016/j.ultras.2019.106017
Received 5 September 2018; Received in revised form 6 September 2019; Accepted 6 September 2019
Available online 06 September 2019
0041-624X/

model. This provides the foundation for optimizing and improving the GMUT in structural design, considering the amplitude prediction and amplitude stability.

Based on the magnetostrictive effect and the magnetization model, the influence of the prestress mechanisms of Terfenol-D and the joint face of the horn on the output amplitude of the GMUT are investigated and are equivalent to two spring-damping systems in series. The vibration equation of the GMUT based on structural kinetics theory is then established and parameters of the GMUT are identified based on impedance analysis. Following this, the mechanical quality factors of the GMUT under different prestress conditions are obtained and the effects of the equivalent stiffness of the prestress mechanism and the joint face of the horn on the prediction of ultrasonic amplitude are studied by nonlinear least square fitting. By analyzing the influence of the prestress of Terfenol-D and the prestress of the joint face of the horn on the ultrasonic amplitude model, the amplitude characteristics of GMUT are investigated. Additionally, an odd power amplitude prediction model (in which the ultrasonic amplitude is related to the odd power terms of the excitation signal) of the GMUT is proposed, considering the effects of the mechanical structure and the excitation signal. This provides reference for further study of the GMUT amplitude model. With different prestress states, the results indicate the possibility of predicting the amplitude output and analyzing the stability of the GMUT under different excitation signals.

2. Theoretical model

2.1. Kinetics model of GMUT

A structural diagram of GMUT is provided in Fig. 1. The ultrasonic oscillator includes a Terfenol-D rod, permanent magnet, magnetic conduction loop, and coil, which generates ultrasonic vibration by the action of excitation signal. The ultrasonic oscillator comes into contact with the vibration unit of the prestress mechanism, transmitting driving force which provides Terfenol-D with prestress. The vibration unit is restrained by the structural stiffness of the prestress mechanism and is connected to the horn by thread. The amplitude of the vibration unit is transmitted and amplified by the horn, and the end of the horn is matched with the cutter. Using this mechanism, the RUM is realized when GMUT rotates.

The properties of the vibration structure of the GMUT are provided in Table 1. Based on this model, the ultrasonic amplitude prediction model of GMUT is established.

In this paper, the interaction between Terfenol-D and external mechanical structure is regarded as the interaction of force, and the mechanical vibration is transmitted by the interaction force. As shown in Fig. 2, the prestress mechanism of Terfenol-D is equivalent to the spring-damping system (k_s, c_s), and the joint face of the horn is equivalent to the spring-damping system (k_c, c_c) [13]. The equivalent kinetics model of GMUT is thus established.

To establish the amplitude prediction model accurately, the vibration unit of the prestress mechanism can be simplified as a particle due to its small mass. The joint face of the horn and the prestress mechanism can be regarded as two single-degree-of-freedom spring-damping systems in series on account of being mostly small enough for the k_s/k_c. A general GMUT amplitude prediction model is then established, which is simplified as shown in Fig. 3.

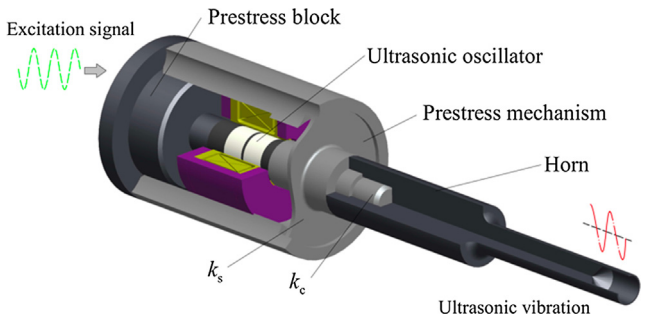

Fig. 1. Structure of GMUT.

Table 1
Vibration structure of the GMUT.

	Property	Unit	
Terfenol-D	Material	/	Tb0.3Dy0.7Fe1.92
	Diameter	mm	13
	Length	mm	16
Prestress mechanism's vibration unit	Material	/	Aluminum
	Mass	kg	0.02
Horn	Material	/	45#
	Mass	kg	0.2
	Length	mm	124

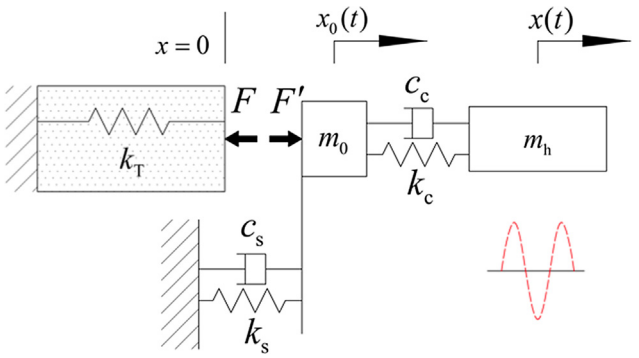

Fig. 2. The equivalent kinetics model of GMUT.

The equivalent stiffness of the vibration system can be obtained by calculation, as shown in Eq. (1).

$$k_{equ} = \frac{k_s k_c}{k_s + k_c} \tag{1}$$

where k_{equ} represents the equivalent stiffness of the mechanical structure, k_s represents the equivalent stiffness of the prestress mechanism, and k_c is the equivalent stiffness of the joint face of the horn.

The vibration unit of the prestress mechanism is always in contact with Terfenol-D during the vibration process. Setting the displacement of the output end of Terfenol-D to zero, the displacement $x_0(t)$ of the vibration unit of the prestress mechanism can be obtained, and is expressed as below:

$$x_0(t) = L_T \varepsilon(t) \tag{2}$$

where L_T represents the effective length of Terfenol-D and $\varepsilon(t)$ represents the total strain of Terfenol-D over time.

Due to the small quality of the prestress mechanism vibration unit, this paper regards the amplitude prediction model as a particle, which means $m_0 \approx 0$. Therefore, Eq. (3) is established by Newton's second law and Hooke's law for m_0.

$$k_s x_0(t) = k_c(x(t) - x_0(t)) \tag{3}$$

The equation is then simplified as below:

$$\begin{cases} x(t) = M_0 x_0(t) = M_0 L_T \varepsilon(t) \\ M_0 = \frac{k_s + k_c}{k_c} \end{cases} \tag{4}$$

where $x(t)$ indicates the input displacement of the horn and M_0 is the vibration transfer factor. Thus, $M_0 = 1$ when k_s/k_c is small enough.

For the horn m_h, the equation can be established by kinetics as shown in Eq. (5).

$$m_h \ddot{x}(t) + c_{equ}\dot{x}(t) + k_{equ}x(t) = F' \tag{5}$$

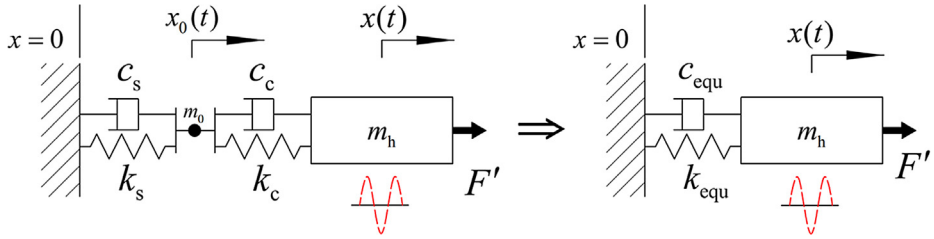

Fig. 3. Simplified GMUT amplitude prediction model.

where m_h denotes the equivalent mass of the horn, c_{equ} is the equivalent damping of the mechanical structure, k_{equ} denotes the equivalent stiffness of the mechanical structure, and $F^{'}$ is the interaction force acting on the horn.

To calculate $F^{'}$, Terfenol-D must be analyzed. As noted in the literature [14,15], the strain composition of Terfenol-D is described as below:

$$\varepsilon(t) = \varepsilon_m(t) + \varepsilon_\lambda(t) \tag{6}$$

where $\varepsilon_m(t)$ indicates elastic strain and $\varepsilon_\lambda(t)$ represents magnetostrictive strain. Young's modulus establishes the relationship between stress and strain as follows:

$$E_T = \left|\frac{\partial\sigma}{\partial\varepsilon}\right| \tag{7}$$

where E_T is Young's modulus of Terfenol-D. Therefore, the stress of Terfenol-D has the following relations:

$$\sigma_d = \sigma - \sigma_0 = E_T\varepsilon(t) - E_T\varepsilon_\lambda(t) - \sigma_0 \tag{8}$$

where σ is the total stress, and σ_d and σ_0 are the dynamic stress and prestress, respectively. Eq. (9) can thus be obtained as:

$$F = \sigma S_T = E_T S_T\varepsilon(t) - E_T S_T\varepsilon_\lambda(t) \tag{9}$$

$F^{'}$ can then be calculated due to the interaction force.

$$F^{'} = -F = E_T S_T\varepsilon_\lambda(t) - E_T S_T\varepsilon(t) \tag{10}$$

Substituting Eqs. (4) and (10) into Eq. (5), the kinetics model of Terfenol-D is obtained as:

$$\frac{M_0 L_T m_h}{E_T S_T}\ddot{\varepsilon}(t) + \frac{M_0 L_T c_{equ}}{E_T S_T}\dot{\varepsilon}(t) + \frac{k_s L_T + E_T S_T}{E_T S_T}\varepsilon(t) = \varepsilon_\lambda(t) \tag{11}$$

2.2. Amplitude prediction model based on magnetization and magnetostriction

The properties of giant magnetostrictive materials have been studied over many years. The effective magnetic field model of the Terfenol-D rod under action of an external exciting magnetic field is provided in reference [16].

$$H_{ef}(t) = H_{ex}(t) + \alpha M(t) \tag{12}$$

where $H_{ex}(t)$ represents the magnetic field generated by an additional excitation signal and $M(t)$ is the magnetization of Terfenol-D. The interpretation of parameter α is given in reference [7].

$$\alpha = \alpha_0 + \frac{9\lambda_s\sigma_0}{2\mu_0 M_s^2} \tag{13}$$

where α_0 characterizes the field induced by the interaction of magnetic moments, $9\lambda_s\sigma_0/(2\mu_0 M_s^2)$ represents the field due to prestress, λ_s and M_s respectively denote saturated magnetostriction and magnetization, μ_0 is vacuum permeability, and σ_0 denotes prestress. Thus, α is affected by prestress acting on Terfenol-D.

The effectiveness of biased magnetic field has been verified [17] to eliminate the frequency doubling effect of Terfenol-D in the high frequency magnetic field. Therefore, $H_{ex}(t)$ can be expressed as Eq. (14):

$$H_{ex}(t) = H_b + N\phi I(t) \tag{14}$$

where H_b represents the bias magnetic field, N is the turns per unit length of the excitation coil, ϕ represents the physical characteristics of the excitation coil which should be determined empirically, and $I(t)$ is the excitation signal.

Without considering the hysteresis effect, the magnetization satisfies the following relation as noted in literature [7]:

$$M(t) = M_s\left[coth\left(\frac{H_{ef}(t)}{a}\right) - \frac{a}{H_{ef}(t)}\right] = M_s\left(\frac{H_{ef}(t)}{3a}\right) + \mathcal{O}\left(\frac{H_{ef}^3(t)}{a^3}\right) \tag{15}$$

where parameter a consists of Boltzmann's constant k_B, the domain density $\mathcal{N}$ and the Boltzmann thermal energy $k_B T$ should be identified due to the unknown $\mathcal{N}$. To facilitate linearizing, high-order terms in the Taylor expansion are neglected, providing:

$$\mathcal{O}\left(\frac{H_{ef}^3(t)}{a^3}\right) \approx 0 \tag{16}$$

Substituting Eqs. (12) and (16) into Eq. (15), formula (17) is obtained as follows:

$$M(t) = \frac{M_s}{3a}(H_{ex}(t) + \alpha M(t)) \tag{17}$$

Which can be written as:

$$M(t) = \frac{M_s}{3a - \alpha M_s}H_{ex}(t) = \frac{M_s H_b}{3a - \alpha M_s} + \frac{M_s N\phi}{3a - \alpha M_s}I(t) \tag{18}$$

To simplify Eq. (18), it is modified as:

$$\begin{cases} M(t) = \frac{M_s}{3a - \alpha M_s}H_{ex}(t) = \frac{M_s H_b}{3a - \alpha M_s} + \frac{M_s N\phi}{3a - \alpha M_s}I(t) = e_1 + e_2 I(t) \\ e_1 = \frac{M_s H_b}{3a - \alpha M_s} \\ e_2 = \frac{M_s N\phi}{3a - \alpha M_s} \end{cases} \tag{19}$$

As noted in the literature [7,18], the relation between magnetostriction and magnetization is described by an empirical magnetostriction model, as shown in Eq. (20):

$$\varepsilon_\lambda(t) = \sum_{i=0}^{\infty}\gamma_i M^{2i}(t),\ i = 0, 1, 2, 3\cdots \tag{20}$$

where $\varepsilon_\lambda(t)$ represents the magnetostriction of Terfenol-D, and γ_i can be obtained by experiments. Eq. (19) is then substituted into (20):

$$\varepsilon_\lambda(t) = \sum_{i=0}^{\infty}\gamma_i(e_1 + e_2 I(t))^{2i},\ i = 0, 1, 2, 3\cdots \tag{21}$$

Eq. (21) shows that the magnetostriction strain of Terfenol-D $\varepsilon_\lambda(t)$ can be expressed as a function of the external excitation signal $I(t)$ for a given GMUT. Note that the parameters e_1 and e_2 are related to the prestress. In most situations the external excitation signal is a sinusoidal alternating current as shown in Eq. (22):

$$I(t) = I_a sin2\pi ft \tag{22}$$

where I_a represents the amplitude of the excitation current and f is the

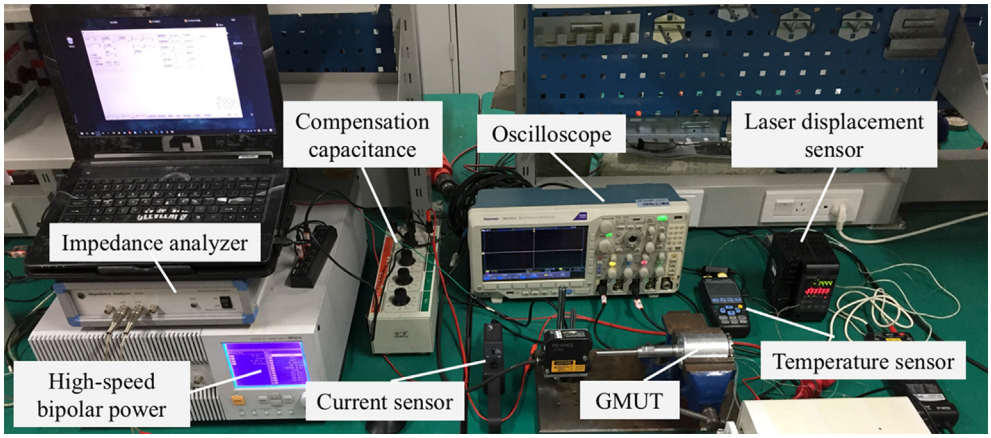

Fig. 4. Experiment apparatus.

frequency of the excitation current. Substituting Eq. (22) into (21) provides:

$$\varepsilon_\lambda(t) = \sum_{i=0}^{\infty} \gamma_i (\epsilon_1 + \epsilon_2 I_a sin2\pi ft)^{2i},\ i = 0, 1, 2, 3\cdots \tag{23}$$

Using the properties of sinusoidal function, Eq. (23) can be decomposed into a fundamental frequency signal composed of $sin2\pi ft$ and its high-order harmonic signal. According to vibration theory, the high-order harmonic component in the damping system exhibits instantaneous attenuation characteristics. In a steady-state vibration, the vibration frequency will be dominated by fundamental frequency signal. The simplified equation is provided below:

$$\varepsilon_\lambda(t) = \eta_0 + \sum_{i=0}^{\infty} \eta_{2i+1} I_a{}^{2i+1} sin2\pi ft,\ i = 0, 1, 2, 3\cdots \tag{24}$$

where η_0 and η_{2i+1}, $i = 0, 1, 2, 3\cdots$ are constants, composed of ϵ_1, ϵ_2, and γ_i, $i = 0, 1, 2, 3\cdots$, and the constant I_a represents the amplitude of the excitation current. The above equations show that the magnetostrictive strain is related to the frequency of the excitation current and the odd power of the amplitude of the excitation current. To obtain the two order vibration system for Terfenol-D, Eq. (24) is substituted into the kinetics differential Eq. (11).

$$\frac{M_0 L_T m_h}{E_T S_T}\ddot{\varepsilon}(t) + \frac{M_0 L_T c_{equ}}{E_T S_T}\dot{\varepsilon}(t) + \frac{k_s L_T + E_T S_T}{E_T S_T}\varepsilon(t) = \eta_0 + \sum_{i=0}^{\infty} \eta_{2i+1} I_a{}^{2i+1} \sin 2\pi ft,\ i = 0, 1, 2, 3\cdots \tag{25}$$

The steady-state solution of the equation is then calculated as follows:

$$\begin{cases} \varepsilon_p(t) = \varepsilon_a \sin(2\pi ft - \varphi) \\ \varepsilon_a = \dfrac{E_T S_T \sum_{i=0}^{\infty} \eta_{2i+1} I_a{}^{2i+1}}{(k_s L_T + E_T S_T)\sqrt{(1-\hbar^2)^2 + (2\varsigma\hbar)^2}} \\ = \dfrac{\sum_{i=0}^{\infty} \eta_{2i+1} I_a{}^{2i+1}}{\left(1 + \frac{k_s}{k_T}\right)\sqrt{(1-\hbar^2)^2 + (2\varsigma\hbar)^2}},\ i = 0, 1, 2, 3 \\ \varsigma = \dfrac{M_0 L_T c_{equ}}{2\sqrt{M_0 L_T m_h (k_s L_T + E_T S_T)}} \\ \hbar = \dfrac{f}{f_r},\ k_T = \dfrac{E_T S_T}{L_T} \end{cases} \tag{26}$$

where ε_a and φ indicate the amplitude and phase of the strain, respectively, ς is damping ratio, $\hbar$ represents frequency ratio, and k_T is the stiffness of Terfenol-D. Taking the amplitude amplification factor as M, the amplitude prediction model of the horn output is shown below:

$$A_a = M\varepsilon_a L_T = \frac{ML_T \sum_{i=0}^{\infty} \eta_{2i+1} I_a{}^{2i+1}}{\left(1 + \frac{k_s}{k_T}\right)\sqrt{(1-\hbar^2)^2 + (2\varsigma\hbar)^2}},\ i = 0, 1, 2, 3\cdots \tag{27}$$

When the ultrasonic vibrator works in resonant state ($\hbar = 1$), the output amplitude prediction model is expressed as follows:

$$\begin{cases} A_r(Q, I_a) = \dfrac{QML_T \sum_{i=0}^{\infty} \eta_{2i+1} I_a{}^{2i+1}}{1 + \frac{k_S}{k_T}} \\ = Q \sum_{i=0}^{\infty} \Re_{2i+1} I_a{}^{2i+1},\ i = 0, 1, 2, 3\cdots \\ \Re_{2i+1} = \dfrac{ML_T \eta_{2i+1}}{1 + \frac{k_S}{k_T}} \end{cases} \tag{28}$$

where $A_r(Q, I_a)$ indicates the amplitude of the resonance state, the mechanical quality factor $Q = 1/2\varsigma$, and ς is damping ratio. Q can also be defined as:

$$Q = \frac{f_r}{f_2 - f_1} \tag{29}$$

where f_1 and f_2 are the half-power frequencies, respectively.

Substituting Eq. (28) into (27), the odd power amplitude prediction model at any frequency is shown below:

$$A(Q, I_a, \hbar) = \frac{A_r(Q, I_a)}{Q\sqrt{(1-\hbar^2)^2 + (2\varsigma\hbar)^2}} = \frac{A_r(Q, I_a)}{\sqrt{[Q(1-\hbar^2)]^2 + \hbar^2}} \tag{30}$$

Note that the parameter $\hbar$ in Eq. (30) is related to the resonance frequency, however, because the effect of Young's modulus can change the resonance frequency [19], the resonance frequency exhibits different resonance frequencies under different excitation currents due to the ΔE effect.

3. Experiments and discussion

3.1. Illustration of experiment apparatus

The experimental apparatus used in this study is shown in Fig. 4. In the experiment, an impedance analyzer (PV80A, Bandera, China) was used to analyze the impedance of GMUT and a high-speed bipolar power supply (BP4610, NF Corporation, Japan) was employed to generate the excitation signals. The excitation signals were monitored by an oscilloscope (MDO3041, Tektronix, USA), and a laser displacement sensor (LK-H008, Keyence, Japan) was used to measure the amplitude at the end of the horn. The sampling frequencies of oscilloscope and the laser displacement sensor were set as 500 kHz and 392 kHz, respectively, and the circuit was compensated by compensation capacitance. The excitation current was then measured using a current sensor. The temperature remained constant throughout the experiments and was monitored by a temperature sensor.

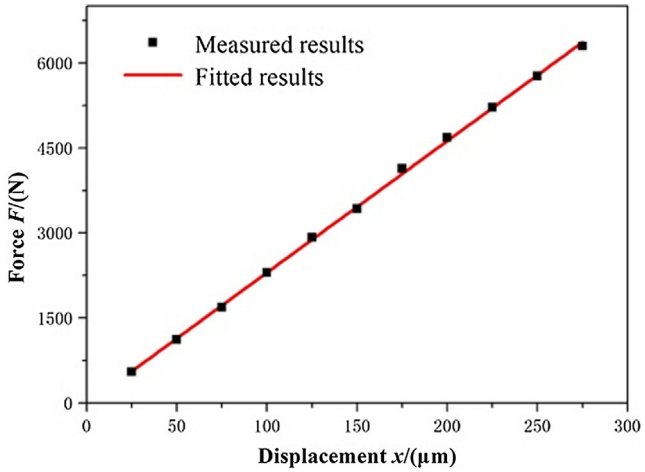

Fig. 5. Fitted and experimental force–displacement response curves of the prestress mechanism's vibration unit.

3.2. Parameter identification

To verify the odd power amplitude prediction model of GMUT, the parameters of the model must be identified. The equivalent stiffness of the prestress mechanism k_s was calculated by measuring the axial displacement of the vibration unit of the prestress mechanism under different forces using a dynamometer and a laser displacement sensor. The results are illustrated in Fig. 5.

According to Fig. 5, the equivalent stiffness of prestress mechanism is calculated as $k_s = 2.322 \times 10^7 N/m$. Using Eq. (1), the relationship between the mechanical equivalent stiffness k_{equ} and the equivalent stiffness k_c of the joint face is then obtained as illustrated in Fig. 6.

As shown in Fig. 6, with the increase of the equivalent stiffness of the joint face k_c, the mechanical equivalent stiffness k_{equ} increases gradually and approaches the equivalent stiffness of the prestress mechanism k_s infinitely. Therefore, with the increase of the torque on the joint face of the horn, the mechanical equivalent stiffness approaches the equivalent stiffness of the prestress mechanism. Fig. 7 illustrates that the resonant frequency and the mechanical quality factor are positively correlated with the torque, indicating that the mechanical quality factor and resonance frequency rise with the increase of torque. This phenomenon can be explained by formula (31) and (32) [9].

$$f_r = \frac{1}{2\pi}\sqrt{\frac{k_{equ} + k_T}{m_h}} \tag{31}$$

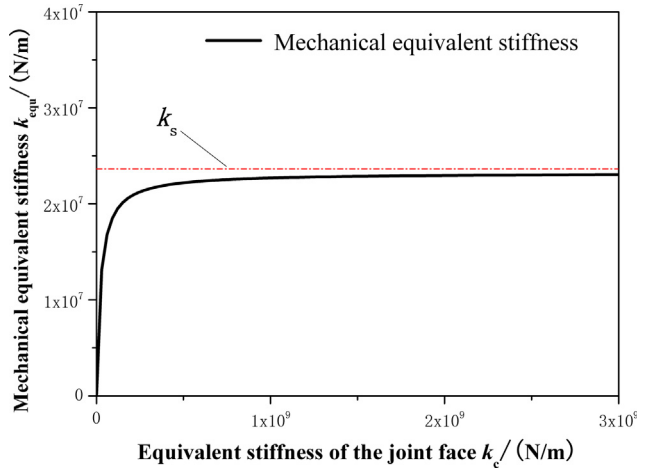

Fig. 6. Relationship between the mechanical equivalent stiffness and the equivalent stiffness of the joint face.

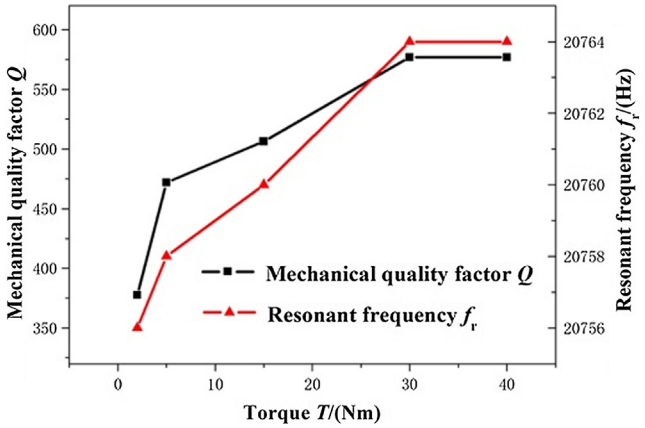

Fig. 7. Mechanical quality factor and resonant frequency-torque curves for the GMUT.

$$c_{equ} = 2m_h\pi(f_2 - f_1) \tag{32}$$

The mechanical equivalent stiffness and the resonance frequency both increase with the increase of torque. However, as Young's modulus of Terfenol-D material is usually dozens of GPa [20], the mechanical equivalent stiffness k_{equ} is smaller than the material stiffness k_T of Terfenol-D. Additionally, because k_{equ} tends to quickly become the equivalent stiffness of prestress mechanism k_s, the resonant frequency increases little and tends to a certain constant. With the increase of torque, the mechanical equivalent damping gradually decreases with a trend to a certain constant, making the mechanical quality factor gradually increase and also tend to a certain constant. It should be noted that changing the torque does not cause a change to the stiffness of Terfenol-D.

When the prestress of Terfenol-D increases, as shown in Fig. 8, the mechanical quality factor increases notably and the resonant frequency increases and tends to a certain value. This is because with the increase of prestress, Terfenol-D is compressed and the material stiffness increases and tends to be stable, however, the mechanical equivalent damping decreases continuously, which makes the mechanical quality factor enlarge sharply.

3.3. Verification of the amplitude prediction model

To verify the amplitude prediction model of GMUT, several prediction experiments were carried out. Firstly, GMUT's amplitude prediction with different mechanical quality factors is realized by changing the torque, because a change of torque will not alter the stiffness of

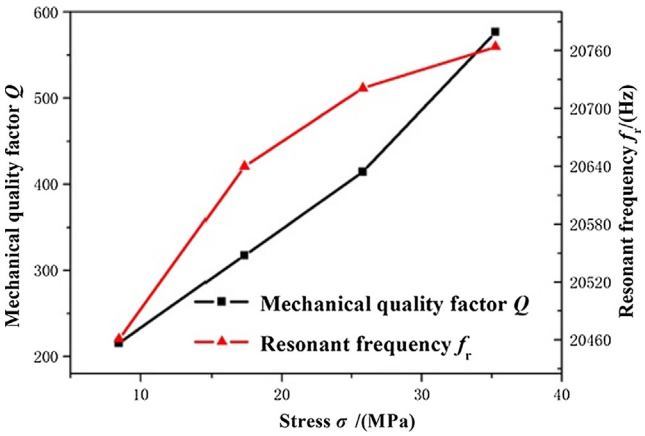

Fig. 8. Mechanical quality factor and resonant frequency-stress curves for the GMUT.

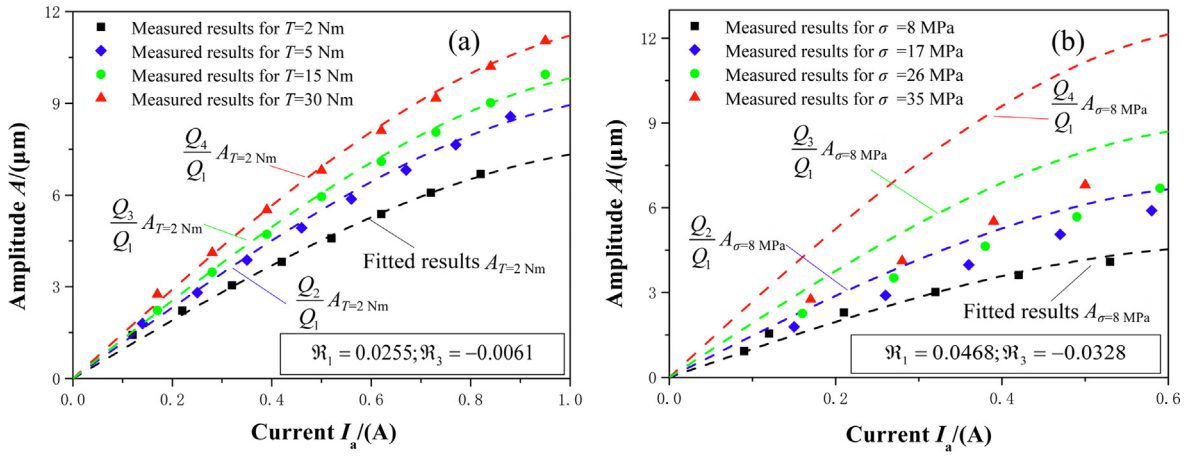

Fig. 9. Amplitude-current response curves: (a) Amplitude-current response curves under four kinds of torque for horn; (b) Amplitude-current response curves under four kinds of prestress for Terfenol-D.

Terfenol-D material and the prestress on the material. Thus, GMUT's amplitude prediction with different mechanical quality factors can be realized by altering the torque. Secondly, variable prestress of Terfenol-D will cause amplitude prediction coefficient $\Re_{2i+1}$ to change in the amplitude prediction model, therefore, the ultrasonic amplitude of GMUT subjected to different prestress must be predicted using nonlinear least square fitting according to the selected number i. The advantages and disadvantages can then be compared.

In the variable torque-amplitude measurement experiment, the mechanical quality factors of four groups for applied torque $T = 2Nm$, $5Nm$, $15Nm$ and $30Nm$ were marked as Q_1, Q_2, Q_3 and Q_4. Then, taking $i = 1$, the fitting curve for measured results for $T = 2Nm$ were obtained, and the prediction coefficients of the amplitude prediction model are $\Re_1 = 0.0255$ and $\Re_3 = -0.0061$, respectively. Marking the fitting curve as $A_{T=2Nm}$, the amplitude prediction curves of other groups can be predicted according to the prediction curves using the mechanical quality factor ratio, as shown in Fig. 9**(a)**. However, in the variable prestress-amplitude test, as shown in Fig. 9**(b)**, the mechanical quality factors for $\sigma = 8MPa, 17MPa, 26MPa$, and $35MPa$ were marked as Q_1, Q_2, Q_3, and Q_4, respectively. The amplitude prediction curves obtained are not able to predict the amplitude of other groups because the prediction coefficients $\Re_{2i+1}$ in the amplitude prediction model are affected by prestress and other factors.

To accurately predict the amplitude at different resonance frequencies, the relationship between the resonance frequency and the excitation current amplitude caused by the ΔE effect is measured. As shown in Fig. 10, Eq. (33) is obtained.

$$\hbar(I_a, f) = \frac{f}{20771 - 30.5I_a} \tag{33}$$

Therefore, for a given GMUT, the impedance analysis is performed as shown in Fig. 11, and the impedance analysis results are shown in Table 2. The corresponding amplitude prediction coefficient $\Re_{2i+1}$ is calculated by selecting different times of i, as shown in Table 3. Curve fitting of the amplitude and amplitude of the excitation current under the resonance condition is then carried out.

According to the parameters in Tables 2 and 3, as well as Eq. (28), and (30), the amplitude prediction models are obtained by i=0,1,2,3 of the given GMUT, as shown in Fig. 12, and the obtained fitting curves have good fitting effect. Therefore, in order to simplify the calculation and predict the amplitude at different frequencies, $i = 0$ is selected to obtain $A_r(I_a) = 10.8251I_a$, which can be substituted into the amplitude prediction model.

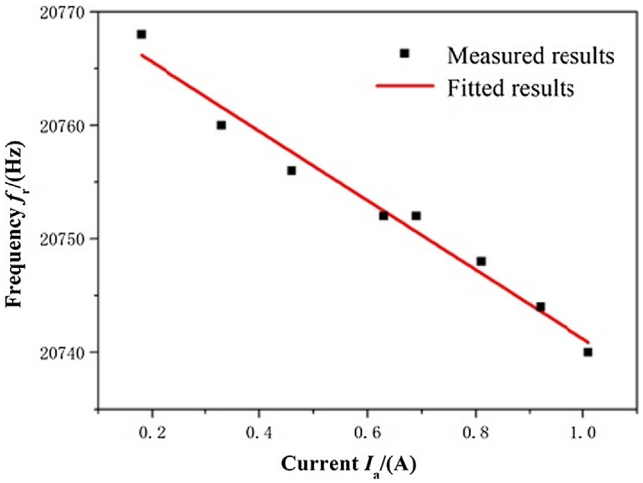

Fig. 10. Amplitude-current response curves at the resonant state of the GMUT.

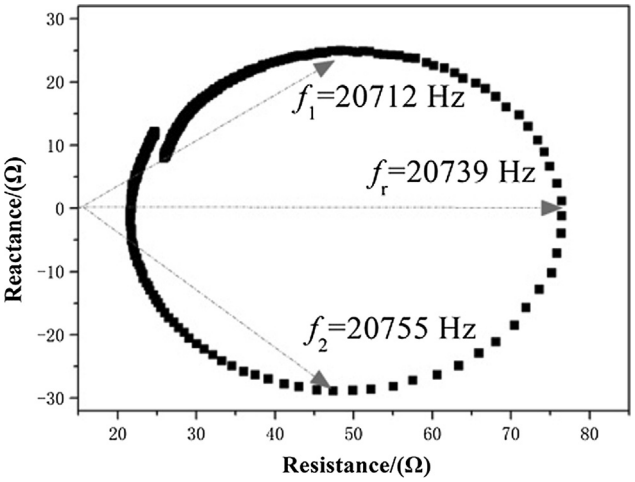

Fig. 11. Impedance circle of the GMUT.

$$A(I_a, f) = \frac{10.8251I_a}{\sqrt{[482.3(1 - \left(\frac{f}{20771 - 30.5I_a}\right)^2)]^2 + (\frac{f}{20771 - 30.5I_a})^2}} \tag{34}$$

Note that when the current increases to a certain extent, the ΔE effect will influence the amplitude prediction coefficient, therefore, the actual current and resonance frequency relationship curve will show a

Table 2
Impedance analysis of the GMUT.

Property	Value
Resonant frequency f_r (Hz)	20,739
Half-power frequency bandwidth $f_2 - f_1$ (Hz)	43
Mechanical quality factor$Q$	482.3

Table 3
Amplitude prediction coefficient of the GMUT.

Item	i	$Q\mathfrak{R}_1$	$Q\mathfrak{R}_3$	$Q\mathfrak{R}_5$	$Q\mathfrak{R}_7$
$Q\mathfrak{R}_{2i+1}$	0	10.8251	/	/	/
	1	10.5042	0.4269	/	/
	2	10.8363	−0.7496	0.8866	/
	3	10.8416	−0.7861	0.9536	−0.0358

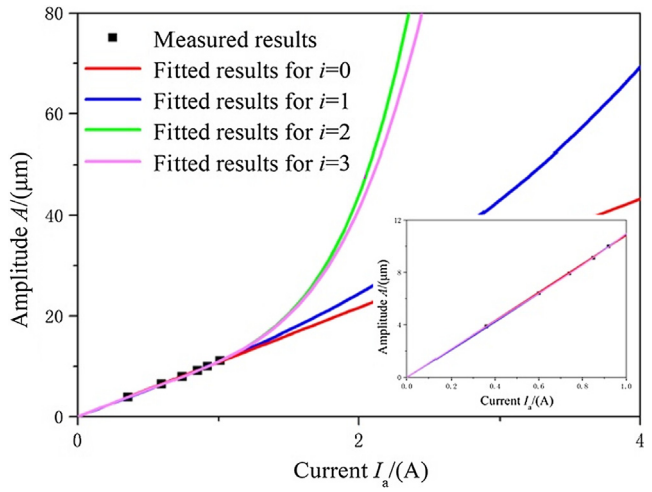

Fig. 12. Amplitude-current response fitting curves with different.i

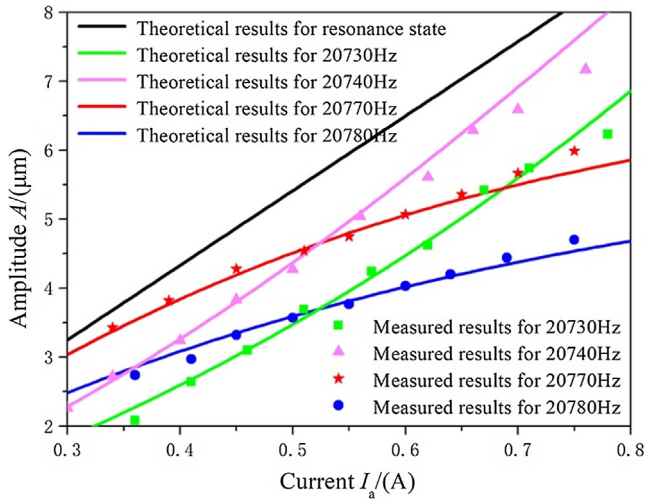

Fig. 13. Amplitude-current response fitting curves at different frequencies.

more complex nonlinear relationship, requiring a higher-order amplitude prediction model. As shown in Fig. 13, the amplitudes obtained at different excitation frequencies are smaller than those at resonant states, and when the excitation frequencies are less than a certain frequency range, the slope of the amplitude prediction curve increases gradually until it is consistent with the slope of the curve at resonant state as the current increases. As the resonance frequency of GMUT decreases gradually and approaches the excitation frequency, the slope of the curve increases gradually, whereas the slope of the curve decreases gradually because it is further away from the excitation frequency.

4. Conclusion

In this paper, kinetics analysis of GMUT was carried out, and a universal quadratic amplitude prediction model based on magnetization and magnetostriction was established. By changing the horn joint face torque and the prestress of Terfenol-D, the mechanical quality factor of GMUT can be modified and the output amplitude can be more effectively adjusted. This provides a new method of optimal design and experimental reference for the study of GMUT. The following conclusions were drawn:

Torque-amplitude experiments illustrated that changing the joint stiffness of the horn can effectively improve the mechanical quality factor, and the output amplitude of the resonance state is proportional to the mechanical quality factor. The accuracy and validity of amplitude prediction can be effectively improved by the appropriate number of terms of the odd power amplitude prediction model.

Due to the ΔE effect, the material stiffness k_T of Terfenol-D will shift during the vibration process, resulting in amplitude prediction error. It is known from the amplitude prediction model that decreasing the equivalent stiffness k_s of the prestress mechanism can minimize the error due to the ΔE effect, and can also increase the vibration amplitude to some extent. The minimum value of k_s is limited by the structure of GMUT itself, which can affect the maximum torque that the horn can achieve and the maximum prestress that Terfenol-D is subjected to, thus limiting the maximum mechanical quality factor of GMUT. Additionally, the greater the mechanical quality factor, the worse the amplitude stability. This presents a relatively optimal engineering design optimization problem.

Experiments on the amplitude of GMUT with excitation signals of different frequencies illustrated that the amplitude increases nonlinearly with the increase of current, and the odd power amplitude prediction model has good applicability and can effectively characterize the vibration performance of GMUT. This further verifies the validity and accuracy of the proposed kinetics model.

Declaration of Competing Interest

The authors declare that they have no known competing financial interests or personal relationships that could have appeared to influence the work reported in this paper.

Acknowledgements

The authors gratefully acknowledged the financial support for this research provided by National Natural Science Foundation of China (Grant No. 51761145103 and Grant No. 51875311) and Shenzhen Foundational Research Project (Subject Layout) (Grant No. JCYJ20160428181916222).

Appendix A. Supplementary material

Supplementary data to this article can be found online at https://doi.org/10.1016/j.ultras.2019.106017.

References

[1] C. Zhang, J. Zhang, P. Feng, Mathematical model for cutting force in rotary ultrasonic face milling of brittle materials, Int. J. Adv. Manuf. Technol. 69 (2013) 161–170, https://doi.org/10.1007/s00170-013-5004-z.
[2] Y. Wang, B. Lin, S. Wang, X. Cao, Study on the system matching of ultrasonic

vibration assisted grinding for hard and brittle materials processing, Int. J. Mach. Tools Manuf 77 (2014) 66–73, https://doi.org/10.1016/j.ijmachtools.2013.11.003.
[3] A.E. Clark, H.S. Belson, Giant room-temperature magnetostrictions in TbFe2 and DyFe2, Phys.rev.b, 5 (1972) 3642–3644. https://doi.org/10.1103/PhysRevB.5.3642.
[4] A.E. Clark, Magnetic and magnetoelastic properties of highly magnetostrictive rare earth-iron laves phase compounds, in, 1974, pp. 1015-1029. https://doi.org/10.1063/1.2947192.
[5] Y. Zhu, J. Liang, Theoretical and experimental investigations of the temperature and thermal deformation of a giant magnetostrictive actuator, Sens. Actuators, A 218 (2014) 167–178, https://doi.org/10.1016/j.sna.2014.07.017.
[6] K.e. Jin, Y. Kou, X. Zheng, The resonance frequency shift characteristic of Terfenol-D rods for magnetostrictive actuators, Smart Mater. Struct. 21 (4) (2012) 045020, https://doi.org/10.1088/0964-1726/21/4/045020.
[7] M.J. Dapino, R.C. Smith, A.B. Flatau, Structural magnetic strain model for magnetostrictive transducers, Magnetics IEEE Trans. 36 (1999) 545–556, https://doi.org/10.1109/20.846217.
[8] W. Huang, B. Wang, S. Cao, Y. Sun, L. Weng, H. Chen, Dynamic strain model with eddy current effects for giant magnetostrictive transducer, IEEE Trans. Magn. 43 (2000) 1381–1384, https://doi.org/10.1109/TMAG.2006.891033.
[9] H. Wakiwaka, M. Lio, M. Nagumo, H. Yamada, Impedance analysis of acoustic vibration element using giant magnetorestrictive material, IEEE Trans. Magn. 28 (1992) 2208–2210, https://doi.org/10.1109/20.179445.
[10] W. Cai, J. Zhang, P. Feng, D. Yu, Z. Wu, A bilateral capacitance compensation method for giant magnetostriction ultrasonic processing system, Int. J. Adv. Manuf. Technol. (2016) 1–9, https://doi.org/10.1007/s00170-016-9602-4.
[11] W. Cai, J. Zhang, D. Yu, P. Feng, J. Wang, A vibration amplitude model for the giant magnetostrictive ultrasonic processing system, J. Intell. Mater. Syst. Struct. 1045389X1771181 (2017), https://doi.org/10.1177/1045389x17711818.
[12] W. Cai, P. Feng, J. Zhang, Z. Wu, D. Yu, Effect of temperature on the performance of a giant magnetostrictive ultrasonic transducer, J. Vibroeng. (2016).
[13] C. Xu, D. Yu, P. Feng, Z. Wu, Modeling method for behaviors prediction of mechanical contacts under nonlinear characteristics, International Bhurban Conference on Applied Sciences and Technology, 2015, pp. 78–83, , https://doi.org/10.1109/IBCAST.2015.7058483.
[14] C. Mungle, C.A. Grimes, W.R. Dreschel, Magnetic field tuning of the frequency-temperature response of a magnetoelastic sensor, Sens. Actuators, A 101 (2002) 143–149, https://doi.org/10.1016/S0924-4247(02)00179-6.
[15] A. García-Arribas, D.D. Cos, J. Gutiérrez, J.M. Barandiarán, Selectable temperature sensitivity of the magnetoelastic resonance, Sens. Actuators A Phys. 106 (2003) 111–116, https://doi.org/10.1016/S0924-4247(03)00146-8.
[16] D.C. Jiles, J.B. Thoelke, M.K. Devine, Numerical determination of hysteresis parameters for the modeling of magnetic properties using the theory of ferromagnetic hysteresis, IEEE Trans. Magn. 28 (1992) 27–35, https://doi.org/10.1109/20.119813.
[17] H. Wakiwaka, M. Nagumo, M. Iio, H. Yamada, Effect of magnetic bias on acoustic vibration element using giant magnetostrictive material, Magn. Japan IEEE Translation J. 8 (1993) 107–111, https://doi.org/10.1109/TJMJ.1993.4565582.
[18] L. Li, D.C. Jiles, Modeling of the magnetomechanical effect: Application of the Rayleigh law to the stress domain, J. Appl. Phys. 93 (2003) 8480–8482, https://doi.org/10.1109/TMAG.2003.815882.
[19] M. Sheykholeslami, Y. Hojjat, M. Ghodsi, K. Kakavand, S. Cinquemani, Investigation of ΔE effect on vibrational behavior of giant magnetostrictive transducers, shock and vibration, 2015, (2015-4-8), Volume 2015 (2015) 1-9. https://doi.org/10.1155/2015/478045.
[20] X.J. Zheng, X.E. Liu, A nonlinear constitutive model for Terfenol-D rods, J. Appl. Phys. 97 (2005) 61, https://doi.org/10.1063/1.1850618.
[21] D. Geng, Y. Liu, Z. Shao, Z. Lu, J. Cai, X. Li, X. Jiang, D. Zhang, Delamination formation, evaluation and suppression during drilling of composite laminates: A review, Compos. Struct. 216 (2019) 168–186, https://doi.org/10.1016/j.compstruct.2019.02.099.